

1 Using large-scale NO<sub>2</sub> data from citizen science for  
2 air quality compliance and policy support

3 *De Craemer Sam<sup>1,2</sup>, Vercauteren Jordy<sup>3</sup>, Fierens Frans<sup>4</sup>, Wouter Lefebvre<sup>2</sup>, Meysman J.R.*

4 *Filip<sup>1,5,\*</sup>*

5 <sup>1</sup> Department of Biology, University of Antwerp, Universiteitsplein 1, B-2610 Wilrijk, Belgium

6 <sup>2</sup> VITO, Boeretang 200, 2400 Mol, Belgium

7 <sup>3</sup> Vlaamse Milieumaatschappij, Kronenburgstraat 45, 2000 Antwerpen, Belgium

8 <sup>4</sup> Belgian Interregional Environment Agency, Gaucheretstraat 92-94, 1030 Brussels, Belgium

9 <sup>5</sup> Department of Biotechnology, Delft University of Technology, Van der Maasweg 9, 2629 HZ

10 Delft, The Netherlands

11  
12 \* Corresponding author: [filip.meysman@uantwerpen.be](mailto:filip.meysman@uantwerpen.be)

13 Abstract: 173 words, Main text : 5115 words, Figures & tables: 1500. Total: 6788

14 **Key words**

15 Air quality, citizen science, nitrogen dioxide, passive sampler, policy support

## 16 Abstract

17 Citizen science projects that monitor air quality have recently drastically expanded in scale.  
18 Projects involving thousands of citizens generate spatially dense datasets using low-cost passive  
19 samplers for nitrogen dioxide (NO<sub>2</sub>), which complement data from the sparse reference network  
20 operated by environmental agencies. However, there is a critical bottleneck in using these citizen-  
21 derived datasets for air quality policy. Passive samplers typically determine the average  
22 concentration over a time span of only a few weeks, and this time-limited character of the  
23 monitoring effort prohibits policy use, as compliance checking requires annual averaged  
24 concentrations, which are not affected by seasonal fluctuations in air quality. Here, we describe a  
25 model approach to reliably transform passive sampler NO<sub>2</sub> data from multi-week averages to  
26 annual averaged values. We verify the assumptions underlying the model procedure, and  
27 demonstrate that model uncertainty complies with the EU quality objectives for air quality  
28 monitoring. Our approach allows a considerable cost-optimization of passive sampler campaigns  
29 and removes a critical bottleneck for citizen-derived data to be used for compliance checking and  
30 air quality policy use.

## 31 1. Introduction

32 Air quality remains an important environmental problem, as 92% of the global population lives  
33 in areas where pollutant levels exceed health-based standards for ambient air quality **(1)**. To  
34 support air quality policies, environmental protection agencies (EPAs) have developed systematic  
35 monitoring programs, which involve a network of reference stations that provide a continuous data  
36 stream for a wide array of air pollutants **(2)**. However, the construction and maintenance of these  
37 reference stations is resource intensive, and hence EPA networks only include a limited number

38 of stations **(3)**. Especially in urban environments, traffic-related air pollution like NO<sub>2</sub> can vary  
39 over small distances **(4–6)**, and so data from a single monitoring station can only be considered  
40 representative of a small surrounding area **(7–9)**. To obtain a more detailed insight into the small-  
41 scale variation of air quality, complementary methods are needed that enable the low-cost  
42 collection of datasets with high spatial resolution. Such spatially dense datasets are critical for the  
43 validation and improvement of air quality models that are used for policy guidance, while they  
44 also allow to investigate the spatial representativeness of the reference stations included in official  
45 monitoring networks **(10,11)**.

46 Passive NO<sub>2</sub> samplers enable the collection of spatially distributed data in cost-efficient manner  
47 **(12)**, while retaining sufficient data quality **(13,14)**, and have been used in local networks of 50-  
48 100 samplers by governmental agencies and researchers to measure NO<sub>2</sub> levels complementary to  
49 reference stations (e.g. **(15–17)**). Very recently, the scale at which these NO<sub>2</sub> passive samplers are  
50 used has greatly expanded, through citizen science projects involving up to 20.0000 participants,  
51 which monitor the air quality outside their house **(18–20)**. However, the policy use of these citizen  
52 science data is currently strongly hampered by the particular way these citizen science projects are  
53 conducted. Citizen-based passive sampler campaigns are typically executed only once, and the  
54 monitoring period is relatively short (e.g. 1-4 weeks for NO<sub>2</sub> in an urban context) to avoid that  
55 passive samplers become saturated **(21)**. Consequently, citizen-derived datasets typically produce  
56 NO<sub>2</sub> concentrations averaged over multiple weeks . In contrast, compliance checking for NO<sub>2</sub> with  
57 guideline values of the World Health Organisation (WHO) or legal limit values requires averaging  
58 periods of 1 hour or 1 year **(22,23)**. Additionally, annual averaged NO<sub>2</sub> values also require a  
59 regularly distributed measurement effort throughout the year **(23)**. Data collected within citizen

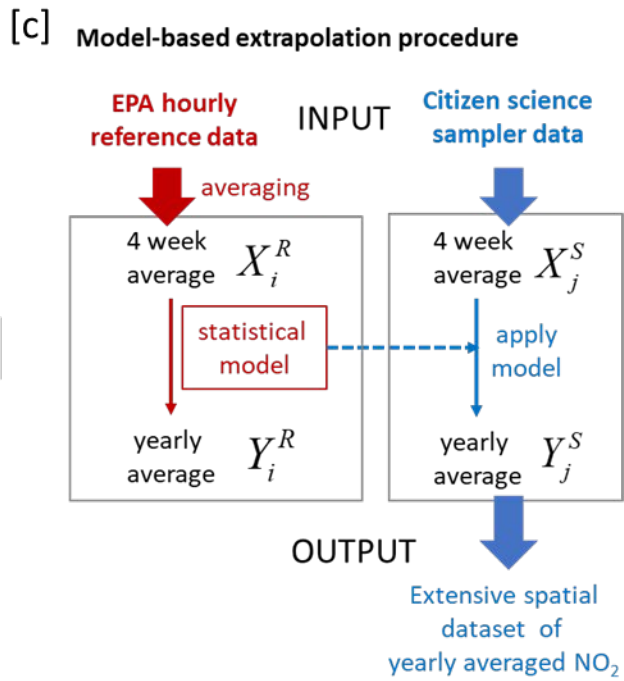
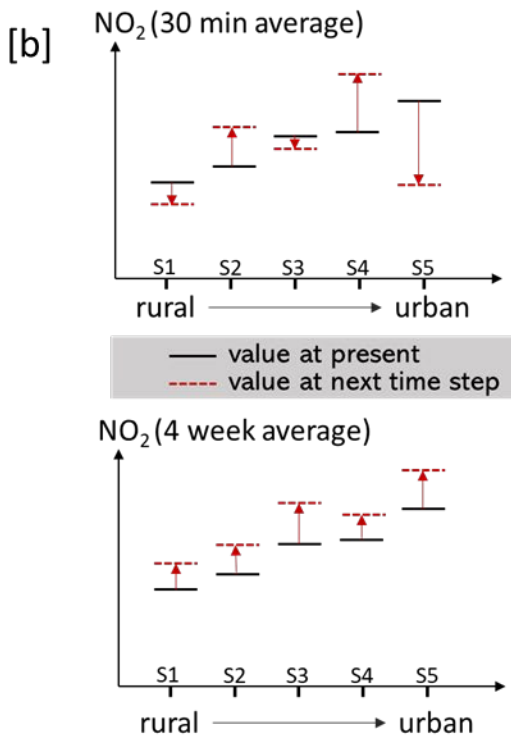
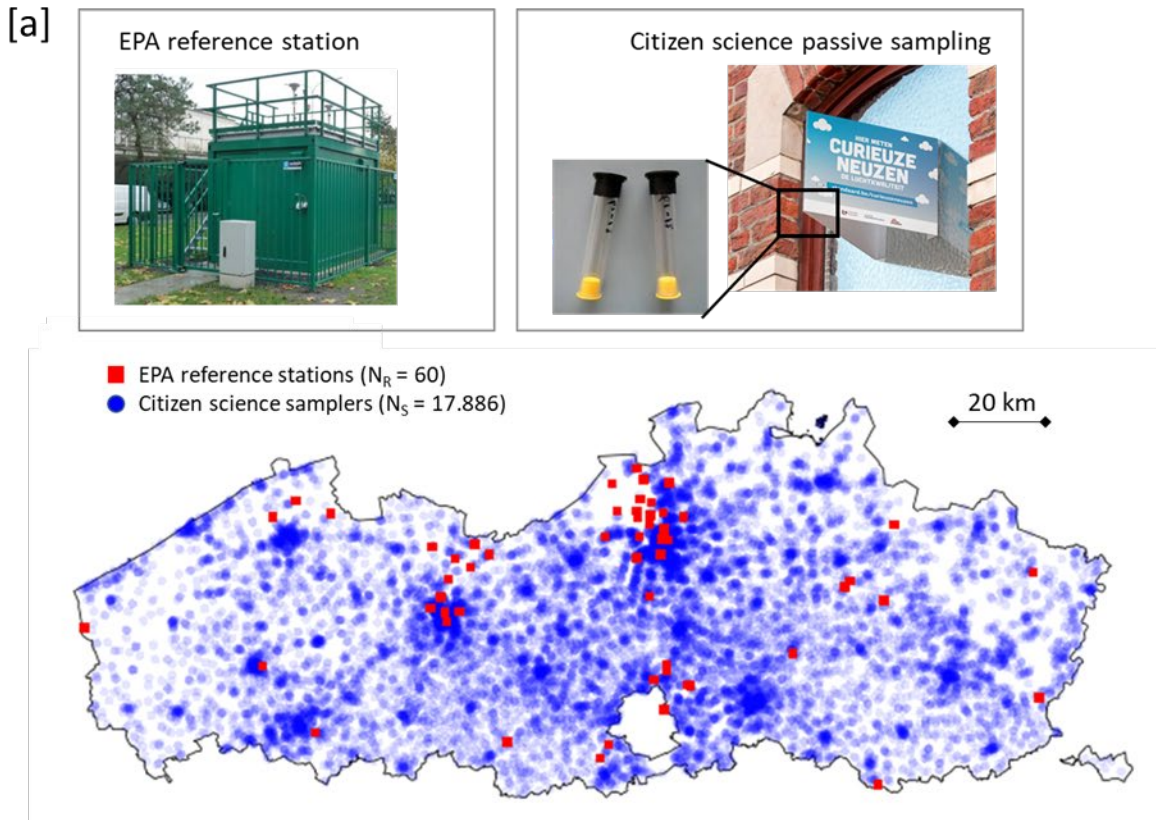
60 science projects do not meet these criteria, and so, these data cannot be directly implemented for  
61 compliance checking.

62 Here, we describe an extrapolation method to obtain annual averages from time-limited NO<sub>2</sub>  
63 passive sampler measurements. Our model approach builds upon previous observations that spatial  
64 patterns of NO<sub>2</sub> remain remarkably stable in time across urban regions (6,16,17,24–26). Different  
65 extrapolation models are tested, and the uncertainty associated with each model approach is  
66 quantified. Additionally, the effect of sampling period on the model uncertainty is evaluated,  
67 allowing insight in the optimal experimental design of sampler campaigns. We evaluate our results  
68 with respect to EU standards for air quality monitoring.

## 69 2. Methods

### 70 2.1. Rationale

71 The rationale of our approach is summarised in Fig. 1. We consider certain a geographical  
72 domain (e.g. city or region) over which air quality is monitored by a network of reference  
73 monitoring stations ( $N_R$  sites), complemented with an additional dense network of passive  
74 samplers ( $N_S$  sites). The reference network is sparse ( $N_R \ll N_S$ ), but provides continuous NO<sub>2</sub> data  
75 at high temporal resolution, which allows to extract both monthly averages ( $X_i^R$  for  $i=1.. N_R$ ) and  
76 annual averages ( $Y_i^R$  for  $i=1.. N_R$ ). The passive sampler network has a high spatial resolution, but  
77 only provides averaged data for over a period of multiple weeks ( $X_j^S$  for  $j=1.. N_S$ ). The objective  
78 is to predict the annual averaged values  $Y_j^S$  based on knowledge of  $X_i^R$ ,  $Y_i^R$  and  $X_j^S$  (Fig. 1c).



80 **Figure 1.** [a] Map showing the  $N_R = 67$  reference stations (red squares) in the monitoring network  
81 of the Flanders Environment Agency across the region of Flanders (Belgium). Additionally, the  
82 map shows the  $N_S = 17.886$  locations at which 4-weekly averaged  $\text{NO}_2$  data were collected in the  
83 citizen science project Curieuzeneuzen via passive samplers (data locations retained after quality  
84 control - blue dots). [b] Schematic illustration of the difference in spatial correlation between both  
85 short-term (30 min averaged) and long-term (4 week averaged)  $\text{NO}_2$  variations. A fictitious  
86 monitoring network consists of 5 stations (S1 to S5) with different  $\text{NO}_2$  levels typifying spatial  
87 variability. Short-term fluctuations show little correlation between stations, while long-term  
88 fluctuations show large correlation. [c] Model-based extrapolation procedure to calculate annual  
89 averaged sampler data from multi-week averaged sampler data.

90

91 As a real world example, Fig. 1a shows the  $N_R = 67$  reference stations in the monitoring network  
92 of the Flanders Environment Agency (Vlaamse Milieumaatschappij, VMM), which are  
93 geographically distributed across the region of Flanders (Belgium). Additionally, Fig. 1a shows  
94 the locations at which 4-weekly averaged  $\text{NO}_2$  data was collected in the Citizen Science project  
95 Curieuzeneuzen in May 2018 ( $N_S = 17.886$  data locations retained after quality control).

96 The starting premise of our model approach is illustrated in a conceptual way in Fig. 1b. The  
97  $\text{NO}_2$  concentration at a given site within a monitoring network is determined by the interplay of  
98 production (e.g. traffic emissions), transport (e.g. upwind supply and dispersal) and removal (e.g.  
99 washout with precipitation or photochemical oxidation). The relative strength of these processes  
100 will differ between sites, thus giving rise to spatial variability (i.e. systematic differences in  $\text{NO}_2$   
101 concentrations between stations S1 to S5). Additionally, the  $\text{NO}_2$  concentration at a given site will  
102 show both short-term and long-term variations, but a critical aspect is that these variations have

103 different drivers. Short-term variations (minutes to days) can be driven by site-specific changes in  
104 local emissions (e.g. a temporary traffic jam) or meteo conditions (e.g. a local rain shower), and  
105 as a result, short-term NO<sub>2</sub> variations will show little correlation between sites (Fig. 1b). In  
106 contrast, the longer-term variations (weeks to years) are mostly driven by changes in weather (e.g.  
107 seasonal variation in atmospheric boundary layer) or economic activity (e.g. summer holidays)  
108 that tend to affect all stations across the domain in a similar manner, so that long-term NO<sub>2</sub>  
109 variations will tend to be correlated between sites (Fig. 1b). Consequently, when averaged over a  
110 sufficiently long period, the site-specific short-time variations will be filtered out, and what  
111 remains are long-term effects that commonly influence all stations. As a result, one expects the  
112 long-term averaged NO<sub>2</sub> levels to move up and down in a synchronous way at different locations,  
113 thus preserving the spatial pattern (Fig. 1b lower panel). Moreover, if a period of a few weeks is  
114 sufficient to filter away short-term effects, one also expects a predictable model relation between  
115 multi-week-averaged and annual averaged NO<sub>2</sub> concentrations that is similar across the whole  
116 monitoring domain (due to temporal stability of inter-site variations). If this is the case, we can use  
117 a model approach that maps multi-week sampler data onto annual averages via the following steps  
118 (Fig. 1c):

- 119 • Determine the time-averaged NO<sub>2</sub> value for the reference stations over the same time  
120 period as passive sampler campaign ( $X_i^R$  data)
- 121 • Determine the time-averaged annual NO<sub>2</sub> value for the reference stations over the year  
122 that contains the passive sampler campaign ( $Y_i^R$  data)
- 123 • Develop a statistical regression model between the independent variable  $X_i^R$  and the  
124 outcome variable  $Y_i^R$  for the  $N_R$  reference stations

- 125           • Apply this same statistical model to the  $N_S$  sampler stations to obtain the annual averaged  
126           estimate  $Y_j^S$  from the available monthly-averaged  $X_j^S$  data for each station in the passive  
127           sampler network. Datasets and model validation

128 We tested this model approach using two datasets collected by the Flanders Environment Agency.  
129 A first dataset includes hourly-averaged  $\text{NO}_2$  concentrations (measured by chemiluminescence)  
130 from the 67 reference stations that make up the regular monitoring network (Fig. 1a). This  
131 “monitor dataset” spans a period of 8 consecutive years from 1 January 2011 to 31 December  
132 2018. We used this dataset to verify whether  $\text{NO}_2$  concentrations at different locations in a  
133 geographical area show similar long-term temporal trends.

134 The second dataset includes  $\text{NO}_2$  concentrations that were obtained via passive samplers (Palmer  
135 diffusion tubes,(12)) over 2-week sampling periods by the Flanders Environment Agency. Passive  
136 samplers were co-located at a subset of 24 stations within the reference monitoring network. This  
137 “sampler” dataset spans a period of 1 year and consists of 26 consecutive measurement periods of  
138 two weeks, lasting from 28 December 2017 until 26 December 2018.  $\text{NO}_2$  sampler data are  
139 reported as the mean of 2-4 replicates at each station and time point. Due to analytical problems,  
140 data from periods 4 and 5 (8 February to 7 March) were not available, thus leaving 24 biweekly  
141 data points at each station. In order to reduce sampler bias,  $\text{NO}_2$  concentrations from passive  
142 samplers were calibrated by orthogonal regression against the data from the reference stations at  
143 which they were co-located (21). We used this “sampler dataset” to validate the model procedure  
144 in a real setting (i.e. with actual passive sampler data). and to verify if and how changes in wind  
145 patterns can compromise the results. To this end, daily data on wind speed and direction for 2018  
146 were obtained from one monitoring station (M802, Havanastraat, Antwerpen) equipped with a  
147 weather station. This allowed comparison of monthly and annual wind patterns.

148 All averages denote arithmetic means over a given time period, and the necessary data  
149 processing and handling of missing data is described in detail in the Supplementary Information.  
150 All data processing and analysis was performed in R 3.6.0. Wind roses were constructed from the  
151 wind speed and direction data using the R package ‘openair’ (27).

## 152 2.2. Model development

153 The extrapolation model seeks a relationship between the average NO<sub>2</sub> concentration measured  
154 over a limited time period (T = 2, 4, 6, 8 weeks) at a given location (the predictor variable X<sub>i</sub> with  
155 i = 1, ..., N<sub>R</sub> the number of stations), and the annual averaged NO<sub>2</sub> concentration from that same  
156 location (Y<sub>i</sub>). Three different models were tested: orthogonal regression, constant off-set and ratio  
157 multiplication. The equations are provided in Sup. Mat. In the orthogonal regression model, the  
158 slope a and intercept b were calculated using Deming regression using the ‘mcreg’ function in the  
159 R package ‘mcr’ (28), assuming equal uncertainties for X<sub>i</sub> and Y<sub>i</sub>. We used the jackknife or leave-  
160 one-out (LOO) method to estimate the model error, implementing the ‘jackknife’ function from  
161 the R package ‘bootstrap’ (29). Air quality directives require that the uncertainty of model  
162 approaches is explicitly quantified (30,31), and associated model quality objectives are typically  
163 expressed as the relative uncertainty at the limit value of a given pollutant (22). The EU air quality  
164 directive defines the model uncertainty as the maximum deviation between the measured and  
165 calculated concentrations for 90 % of monitoring points, and specifies that this uncertainty should  
166 be less than 30% for annual NO<sub>2</sub> values, defined at the limit value C<sub>lim</sub> = 40 µg/m<sup>3</sup> (22). To verify  
167 whether our model meets the EU model quality objectives, we quantified the model uncertainty as  
168 the P90 value of the frequency distribution of residuals  $\varepsilon_{i,p}^R(T, M)$  divided by C<sub>lim</sub> (see Sup. Mat.  
169 for a definition of residuals and model errors).

170

## 171 3. Results

### 172 3.1. Model assumptions

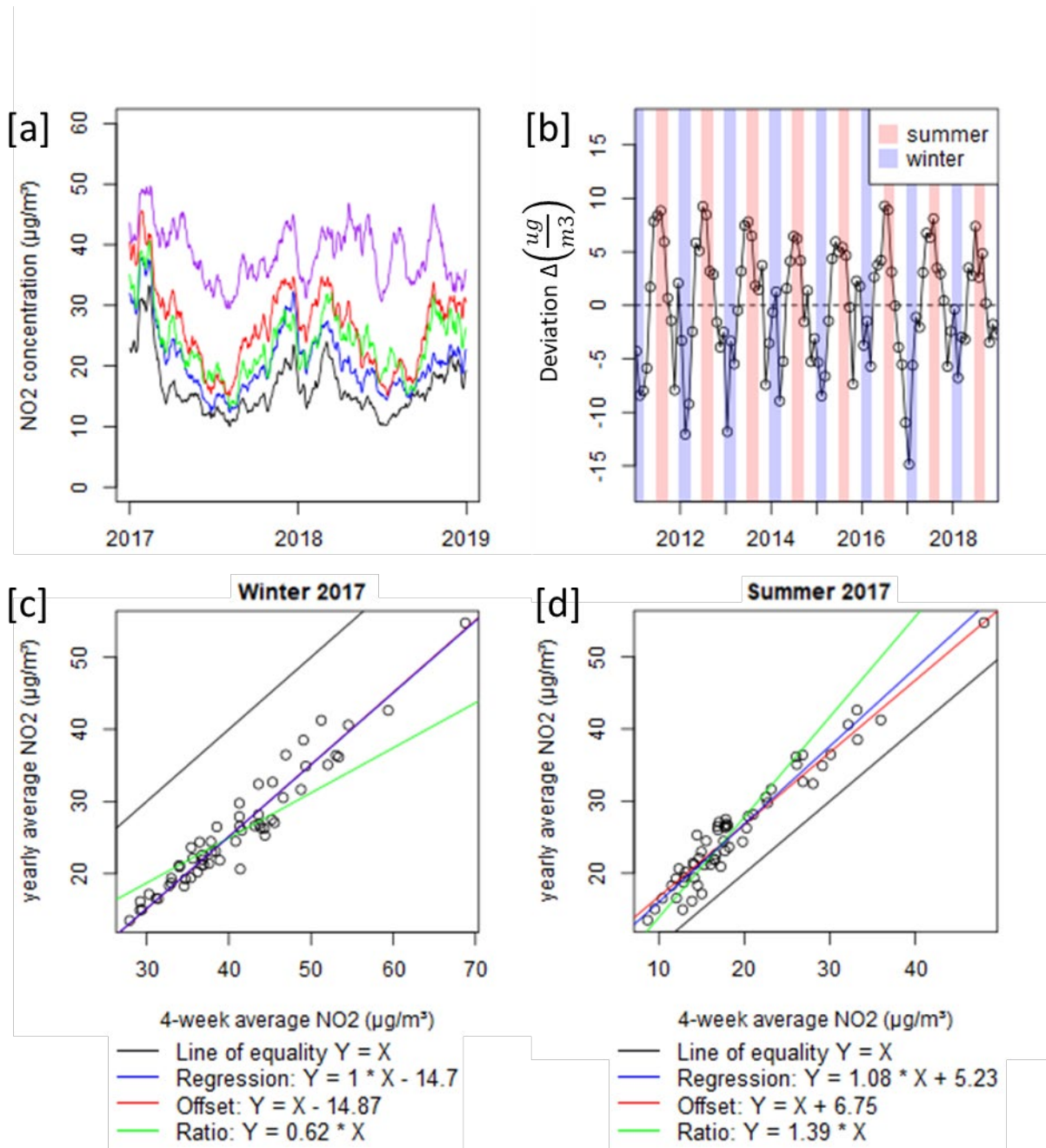
173 The central assumption of our extrapolation approach is that ambient NO<sub>2</sub> shows spatial  
174 synchrony when averaged over a multiple weeks, i.e. the relative concentration differences  
175 between locations within the study area remain stable in time. Figure 2a examines this idea of  
176 spatial synchrony for NO<sub>2</sub> data obtained from the reference stations in the official monitoring  
177 network in the region of Flanders (Belgium). It shows a two-year time series from reference  
178 stations that are situated in different geographical locations and cover a range of emissions and  
179 concentrations levels (countryside, urban, industrial). Comparison of the 4-week moving averages  
180 reveals considerable covariation in time between the stations (for clarity only 5 stations are  
181 displayed; a plot for all 67 available stations over the whole 8-year period shows the same  
182 behaviour – Fig. S1a). Spatial synchrony becomes even more apparent when the concentration at  
183 each site is normalised (as  $X_i - \bar{X}_i$ , where  $\bar{X}_i$  is mean over the whole 8-year period at station  $i$ ).  
184 The normalized concentrations at all 67 stations display a similar seasonal pattern and slowly  
185 decreasing trend with time (Fig. S1b).

186 Time series analysis shows that spatial synchrony becomes stronger as the integration period of  
187 the passive sampler become longer. To demonstrate this, we performed a pair-wise comparison of  
188 the time series of all stations **(32)**, after adopting a moving average that broadly encompasses the  
189 measurement period of passive samplers (Fig. S2). The average Pearson correlation across all  
190 station pairs rapidly increases from 1 day to 7 day averaging, as short term fluctuations are filtered  
191 away. Subsequently, the correlation increases more slowly. Pairwise t-tests (in which the degrees  
192 of freedom were reduced for temporal autocorrelation with a lag period of 365 days) show that the  
193 correlation was significant for 98.5% of the pairs at an averaging period of 4-weeks .

194 The dominant frequency component in the NO<sub>2</sub> data from the reference stations is the seasonal  
195 cycle. Figure 2b shows the evolution over eight years of the deviation between the inter-site mean  
196 of annual averages and 4-week averages, i.e.,  $\Delta = \langle Y_i^R \rangle - \langle X_{i,p}^R \rangle$ , where the operator  $\langle \rangle$  takes the  
197 arithmetic mean over all stations. The deviation  $\Delta$  shows a clear seasonal cycle, where 4-week  
198 averaged NO<sub>2</sub> levels in summer are lower compared to the annual average, while they exceed the  
199 annual average in winter. The underlying mechanism is likely meteorology (more stable  
200 atmospheric conditions with less dispersion) and increased emissions that favour higher  
201 concentrations in winter months compared to the annual average, and lower concentrations in  
202 summer (33). The reference station that shows the least covariation with other stations is situated  
203 at an oil refinery in the harbour of Antwerp (purple curve in Figure 2a). This is not unexpected, as  
204 industries at different locations may show different temporal economic activity and associated  
205 emissions patterns, thus diminishing covariation. Overall however, the temporal covariation of this  
206 industrial station with urban and residential stations remains substantial, suggesting that region-  
207 wide changes in meteorology remain an important driver at this industrial station.

208 The fact that the NO<sub>2</sub> data are spatially synchronous suggests that there could be a strong  
209 correlation between multi-week averaged values  $X_i^R$  and annual averaged values  $Y_i^R$  for the  
210 reference monitoring stations, regardless of the time of year. This is indeed the case, as illustrated  
211 in Figure 2c-d for two separate 4-week periods, respectively in the winter and summer of 2017.  
212 For all reference stations in the official monitoring network with available data ( $N_R = 57$  stations),  
213 the multi-week-average  $X_i^R$  is plotted versus the year-average  $Y_i^R$  over 2017. The  $X_i^R$  and  $Y_i^R$   
214 values show a high correlation (Pearson R: 0.962 in winter, 0.968 in summer) and the best fit of  
215 the regression, offset and ratio models are shown. In winter the data fall below the 1:1 line  
216 (negative  $\Delta$ ), while in summer one has the opposite situation (positive  $\Delta$ ). These examples are

217 highly representative for other periods in the 8 year data series. In all instances the data show a  
 218 clear linear relationship between multi-week-averaged and annual averaged NO<sub>2</sub> data (mean  
 219 Pearson R = 0.961 over all n=103 periods; range 0.88-0.99; Fig. S3).



220

221 **Figure 2.** [a] NO<sub>2</sub> time series over 2 consecutive years at 5 stations selected from the reference  
 222 monitoring network in Flanders. The curves denote the 4-week moving average of hourly NO<sub>2</sub>

223 data. [b] The deviation between annual averaged NO<sub>2</sub> values and 4-week averages across the  
224 reference monitoring network over 8 consecutive years. The deviation  $\Delta = \langle Y_i^R \rangle - \langle X_{i,p}^R \rangle$  takes  
225 the mean over all  $N_R = 67$  stations in the network. Winter (Dec 21 to Mar 20) and summer (21 Jun  
226 to 20 Sept) are shown in blue and red shading respectively. [c-d] Scatterplots of NO<sub>2</sub> data for NR  
227 = 67 reference stations showing 4-week averages against annual averages for 2017 in [c] winter  
228 (period 1 of 2017) and [d] summer (period 6 of 2017). Dashed line denotes 1:1 equality. Solid lines  
229 denote model fits.

### 230 3.2. Model comparison

231 Our analysis hence suggests that multi-week-averaged NO<sub>2</sub> data can be predictably extrapolated  
232 to annual averaged values. So, what extrapolation model performs best? Table 1 depicts the overall  
233 model performance for the three models (M = Regression, Offset and Ratio) as a function of the  
234 averaging period (T = 2, 4, 6 or 8 weeks). Irrespective of the averaging period T, the Regression  
235 model performs best (lowest RMSE), closely followed by the Offset model, while the Ratio model  
236 gives a substantially higher RMSE in all cases. For all models, an increase in the length of the  
237 averaging period T increases the model performance. The largest decrease in RMSE is realized  
238 when going from 2 to 4 weeks, whereas subsequent increases in T have a smaller effect, which is  
239 congruent with how the co-variation between stations depends upon the measurement period of  
240 passive samplers (Fig. S2).

241 **Table 1.** Summary of model-based extrapolation approach applied to the monitor dataset (upper  
242 part) and sampler dataset (lower part). A model-data comparison is performed for three different  
243 statistical models (Regression, Offset, Ratio) and for different averaging periods (T). The Root  
244 Mean Square Error (RMSE) and model uncertainty are tabulated. See paragraph 2.2 for  
245 mathematical formulae.

Monitor dataset		Regression		Offset		Ratio	
Period T (weeks)	# periods	RMSE ( $\mu\text{g}/\text{m}^3$ )	Uncertainty (%)	RMSE ( $\mu\text{g}/\text{m}^3$ )	Uncertainty (%)	RMSE ( $\mu\text{g}/\text{m}^3$ )	Uncertainty (%)
2	206	2.8	11.2	3.0	12.0	3.7	14.3
4	103	2.2	9.0	2.3	9.5	3.0	11.4
6	64	2.0	8.1	2.1	8.5	2.7	10.2
8	48	1.8	7.5	1.9	7.5	2.6	9.6

Sampler dataset		Regression		Offset		Ratio	
Period T (weeks)	# periods	RMSE ( $\mu\text{g}/\text{m}^3$ )	Uncertainty (%)	RMSE ( $\mu\text{g}/\text{m}^3$ )	Uncertainty (%)	RMSE ( $\mu\text{g}/\text{m}^3$ )	Uncertainty (%)
2	24	3.5	13.1	3.5	13.7	4.3	16.2
4	11	2.8	11.0	2.9	11.7	3.7	14.1
6	8	2.4	9.4	2.5	10.9	3.3	13.2
8	5	2.2	9.6	2.3	9.7	2.9	11.1

246

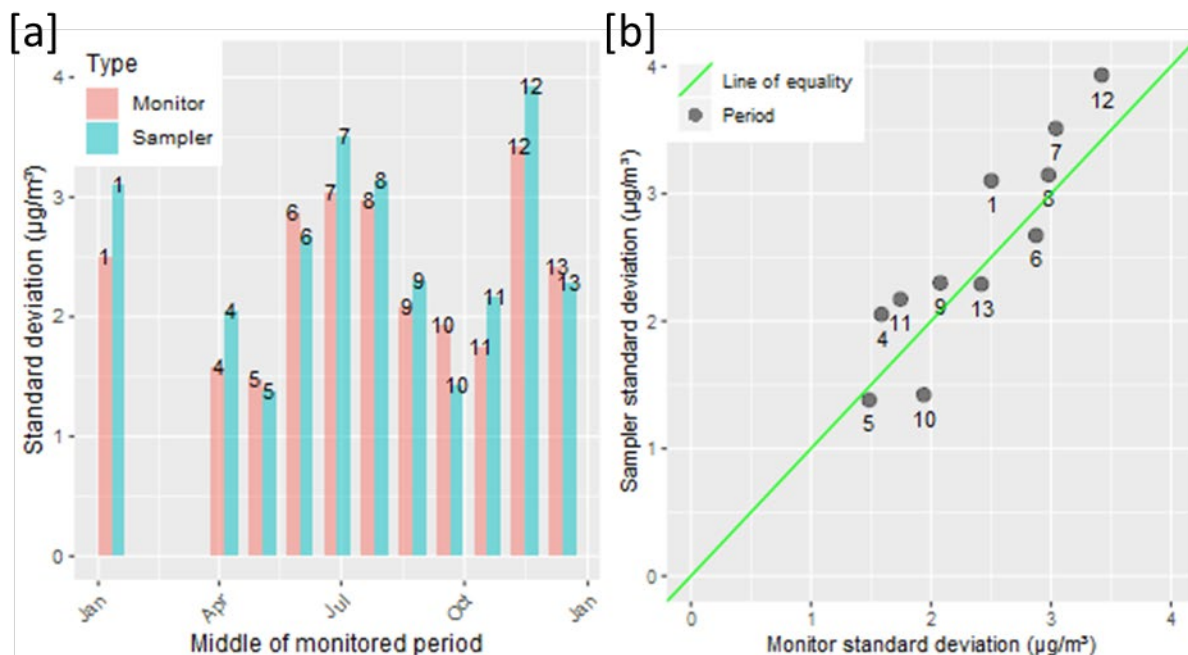
247 Normal Q-Q plots reveal that the residuals from the Regression and Offset models are normally  
 248 distributed, while the residuals of the Ratio model show tailing to the right (Fig. S4). Furthermore,  
 249 analysis of variance (ANOVA) on the monitoring dataset shows that the residuals do not depend  
 250 on the averaging period T, the year or their interaction ( $P>0.9$  for all associations). The model  
 251 uncertainty for the three models ranges between 7.5% and 11.2%, well below the model quality  
 252 objective of 30% as specified in the EU directive (Table 1).

### 253 3.3. Model application to sampler data

254 Until now our analysis has been exclusively based on  $\text{NO}_2$  data obtained from reference  
 255 monitoring stations. In real life however, the extrapolation procedure will principally target data  
 256 obtained from passive sampler deployments. To verify whether this makes a difference, we

257 investigated a data series of one year (13 consecutive periods of 4 weeks over the year 2018) where  
258 both reference monitor data and passive sampler data were collected at the same location ( $N_S = 24$   
259 stations). We implemented the Regression, Offset and Ratio models to calculate the year-averaged  
260 values  $Y_{i,p}^{S,model}(T, M)$  and compared these values the corresponding year-averaged values  $Y_i^{S,true}$   
261 as derived by directly averaging the sampler data. Model results are highly similar to above (Table  
262 1). Irrespective of the averaging period  $T$ , the Regression model performs best, closely followed  
263 by the Offset model. Model uncertainties are slightly higher than above (9.3-13.6%), but still fall  
264 well below the 30% model quality objective of the EU directive.

265 The model uncertainty in Table 1 is calculated from the model errors  $\sigma_p^S(T, M)$ , which require  
266 a year-long coverage of sampler data. In real-world applications however, sampler campaigns will  
267 only be conducted at a single instance, and not over a whole year. As a consequence, one cannot  
268 determine the model error  $\sigma_p^S(T, M)$  directly. Still, when reference data are available, one can  
269 calculate the model error  $\sigma_p^R(T, M)$  via the LOO approach, and then use the resulting value as an  
270 estimate for  $\sigma_p^S(T, M)$ . To evaluate this, Figure 3a compares the corresponding model errors  
271  $\sigma_p^R(T, M)$  and  $\sigma_p^S(T, M)$  for each time period of 4 weeks (residuals for all individual stations are  
272 shown in Fig. S5). The monitor-based and sampler-based model errors are of similar magnitude  
273 (ranging between 1 and 4  $\mu\text{g}/\text{m}^3$ ) and show the same temporal trend across the different  
274 measurements periods (Fig. 3a). Moreover, there is an excellent linear relation between both model  
275 errors (Fig. 3b), showing that  $\sigma_p^R(T, M)$  indeed provides a good estimate of the sought-after model  
276 error  $\sigma_p^S(T, M)$ . Consequently, the LOO approach based on monitor data provides an appropriate  
277 way to estimate the model uncertainty when performing the model extrapolation on sampler data.  
278



279  
 280 **Figure 3.** [a] Model errors from the orthogonal regression model as derived from both the sampler  
 281 dataset  $\sigma_p^S(T, M)$  (green bars) and as derived from the monitor dataset by the LOO approach  
 282  $\sigma_p^R(T, M)$  (red bars). Values are plotted for each 4-week period in 2018. Data for periods 2 and 3  
 283 are missing. [b] Scatterplot of model errors as derived from sampler and monitor datasets. Solid  
 284 line denotes 1:1 equality. Numbers indicate the 4-week period.

### 285 3.4. Wind effects

286 The above results demonstrate that multi-week  $\text{NO}_2$  sampler data can be predictably extrapolated  
 287 to annual averaged values, and that this can be achieved with a relative small uncertainty ( $< 11\%$   
 288 at  $T = 4$  weeks). An important question is whether there are conditions where this model-based  
 289 extrapolation may induce large errors? In the 2018 passive sampling campaign, the largest residual  
 290  $\varepsilon_{i,p}^S(T, M)$  was obtained in period  $p = 12$  at station R804 ( $M = \text{Regression}$ ,  $T = 4$  week). The  
 291 measured annual  $\text{NO}_2$  concentration at this station was  $15 \mu\text{g}/\text{m}^3$  higher than the model-predicted  
 292 value from this period (Fig. S5), and this residual was outside the 95% confidence interval of  $\pm$

293 5.6  $\mu\text{g}/\text{m}^3$ . A closer inspection of the positioning and wind dynamics provides an explanation for  
294 this high deviation. Station R804 is situated immediately east of the R1 Ring Road, which is the  
295 stretch of highway with the highest traffic intensity in Flanders (Fig. S6). Period 12 had an  
296 unusually high proportion of easterly winds compared to the average wind pattern for 2018 (winds  
297 from the southwest are dominant), which transport the high emissions from the highway away  
298 from the monitoring station, thus explaining the observed underestimation of the annual averaged  
299  $\text{NO}_2$  concentration. Accordingly, in stations located close to strong emissions sources, the wind  
300 regime during the measurement period should be suitably representative to avoid large  
301 extrapolation errors. To counteract bias at such locations, the sampling design could be adapted  
302 and multiple samplers could be positioned around the emission source (e.g. upwind and downwind  
303 locations).

#### 304 4. Discussion

305 Recently, large-scale citizen science projects involving thousands of participants have generated  
306 extensive  $\text{NO}_2$  datasets via passive samplers (18–20,34). These datasets typically assess the  
307 averaged air quality over a limited time period (1-4 weeks), and could provide a valuable  
308 contribution to air quality policy, provided the data can be reliably upscaled to year-averaged  
309 values. Here, we have evaluated a procedure to reliably extrapolate the time-limited results of  $\text{NO}_2$   
310 passive samplers from multi-week to annual averaged values. Note that this approach implies an  
311 inversion of the traditional approach to air quality monitoring. Conventionally, the temporal  
312 variation of air quality is characterized in detail via reference stations, and subsequently, suitable  
313 spatial extrapolation occurs via geo-spatial interpolation, LUR or atmospheric dispersion models  
314 (35). In the procedure developed here, one first characterizes the air quality in high spatial detail

315 using citizen-based monitoring, and subsequently, one extrapolates these data in time to arrive at  
316 annual averages, which can then be used for compliance checking.

#### 317 4.1. Spatial synchrony in NO<sub>2</sub> data

318 The central premise of our model procedure is that air quality shows spatial synchrony: when  
319 averaged over a suitably long period, sampling locations will preserve the spatial pattern in NO<sub>2</sub>  
320 concentrations, when assessed at different times. Early work with NO<sub>2</sub> passive samplers (2 week  
321 averages) already noted that areas with high pollution tend to remain polluted, and that sites rank  
322 in the same order during repeated surveys, although the absolute NO<sub>2</sub> concentrations may vary  
323 (17). This temporal stability of spatial contrasts was corroborated in follow-up studies (6,16,17,24–  
324 26). Our statistical analysis of an 8-year NO<sub>2</sub> data series from the reference stations in the official  
325 monitoring network of Flanders (Belgium) confirms the existence of strong spatial synchrony, but  
326 additionally demonstrates that spatial synchrony increases with the integration period of the  
327 samplers (Fig. S2). Reference stations that are situated in different geographical locations and  
328 different emission regimes (countryside, urban, industrial) show a similar temporal variation, when  
329 short-term fluctuations are filtered away (Figure 2; Fig. S1). This indicates that the key drivers of  
330 longer-term NO<sub>2</sub> variation must act in a synchronous manner across the whole region. Such drivers  
331 could include region-wide changes in economic activity that synchronize traffic NO<sub>2</sub> emissions,  
332 seasonal patterns in heating activity and household emissions, as well as seasonal variation in the  
333 structure of the atmospheric boundary layer, which could synchronize changes in dispersal  
334 between locations. Given this, we expect the spatial synchronicity to hold on a scale of a city,  
335 region or small country, but to break down on the larger scale of a large country or a continent.  
336 Our finding that spatial contrasts in pollutant concentrations remain stable over a time span of 8  
337 years, is of particular importance for the development of land-use regression (LUR) models, which

338 provide a cost-effective approach for predicting the air quality at sites not covered by reference  
339 networks (36,37). LUR models have been widely used in epidemiological studies and are often  
340 applied to time periods before (hindcasting) or after (forecasting) the period of air quality  
341 monitoring used in model development. The spatial synchrony as observed in our data justifies the  
342 temporal stability of LUR models, thus increasing their predictive power and reliability (24–26).

#### 343 4.2. Model-based extrapolation to annual NO<sub>2</sub> concentrations

344 Spatial synchrony of NO<sub>2</sub> data has an important additional advantage: it implies that there is a  
345 good correlation between multi-week-averaged NO<sub>2</sub> values and annual averaged values NO<sub>2</sub> for  
346 sampling stations within a wider region. This property has been occasionally employed to adjust  
347 passive sampler data for seasonal variability (38), but its validity has not been systematically  
348 investigated. Here, we evaluated three different models to assess this correlation and estimated the  
349 model uncertainty associated with each of these models. The orthogonal regression model  
350 performs best overall though it is closely followed by the constant offset model, while the Ratio  
351 model performs less well. The orthogonal regression model systematically shows a 1:1 slope and  
352 a non-zero offset, hence explaining the similar performance of the Regression and Offset models.  
353 This “offset” response is consistently observed throughout the 8 year long time series (Figure 2 c-  
354 d), and has been casually reported in passive sampler studies (16,38). To explain this, one needs a  
355 process that affects countryside locations (low NO<sub>2</sub>) and urban stations (high NO<sub>2</sub>) in the same  
356 absolute manner, i.e., by subtraction or addition of a similar concentration difference. A simple  
357 seasonal change in the ventilation rate of the atmospheric boundary layer cannot account for this,  
358 as this would change the slope, but would not create an offset. One option is that seasonal weather  
359 patterns predominantly influence the regional background, with lower NO<sub>2</sub> values in summer  
360 compared to winter due to e.g. an expanded atmospheric boundary layer and increased

361 photochemical oxidation of NO<sub>2</sub> in summer (Fig. 2b). This would affect all stations in a similar  
362 fashion, thus explaining the offset seen in the relation between multi-week-averaged and annual  
363 averaged NO<sub>2</sub> values (Figure 2c-d).

364 Our analysis demonstrates that the extrapolation from multi-week-averaged to annual averaged  
365 NO<sub>2</sub> values works well in the majority of cases. Still, there are a number of specific circumstances  
366 where the approach may lead to biased results. Locations that are heavily influenced by variable  
367 industrial emissions need not be synchronous with other locations (Figure 2a). Another point of  
368 attention are locations with a major nearby pollution source (e.g. stations near high traffic  
369 intensities) exposed to non-representative wind conditions. These locations may show strong  
370 underestimation or overestimation, depending on the direction of the wind (Fig. S6). More  
371 generally, the extrapolation of passive sampler data can be biased when the emission source  
372 contributions and meteorological conditions during the measurement period are not representative  
373 for the year over which the extrapolation occurs. Accordingly, one should scrutinize for local  
374 abnormalities in meteo-conditions and source emissions, for example, when the traffic intensity  
375 deviates at a given location during the measurement period (e.g. due to road works).

#### 376 4.3. Cost-efficient design of passive sampler campaigns

377 In addition to citizen science, low-cost passive sampler approaches are also widely employed by  
378 EPA's to identify localized hotspots or to complement the existing measurement network in a cost-  
379 efficient manner (4,16). To meet with the data quality objectives for ambient air quality  
380 assessment, passive sampler campaigns are typically repeated throughout the year to ensure full  
381 time coverage (e.g. 12 consecutive monthly passive sampler campaigns). However, this is labour  
382 intensive, and so the capability to reliably extrapolate the data for a multi-week single to a annual  
383 averaged value – as proposed here - implies a substantial gain in terms of cost efficiency. The

384 extrapolation approach thus allows to increase the number of measurement locations by a factor  
385 of 12 for the same deployment effort (i.e. for the same amount of passive samplers analysed).

386 Our results provide some valuable guidelines for the optimal experimental design of passive  
387 sampler campaigns. Table 1 shows the model uncertainty as a function of the measurement period  
388 ( $T = 2, 4, 6, 8$  weeks). The model uncertainty decreases for longer measurement periods, as  
389 emissions and meteorology will show higher spatial synchrony when averaged over a longer period  
390 (Fig. S2). When increasing  $T$  from 2 to 4 weeks, the model uncertainty substantially decreases, but  
391 after that, the further improvement of the model uncertainty is marginal.

392 A critical concern with passive sampler measurements for longer periods is the saturation of the  
393 samplers. For example,  $\text{NO}_2$  diffusion tubes typically saturate after 4 weeks at urban traffic stations  
394 with daily  $\text{NO}_2$  values  $> 50 \mu\text{g}/\text{m}^3$ . Deployment of these samplers over 2 weeks requires a similar  
395 effort than deployment over 4 weeks (both require one single campaign), but due to the risk of  
396 saturation, deployment over 6 or 8 weeks necessitates a doubling of the effort (2 consecutive  
397 campaigns are needed). Accordingly, 4-week deployment seems to be an optimal balance  
398 (enlarging  $T$  to reduce model uncertainty while avoiding the risk of saturation).

#### 399 [4.4. Compliance with EU legislation](#)

400 The spatially dense datasets resulting from large-scale citizen science projects complement the  
401 data resulting from the sparse official networks of reference monitor stations. But to what extent  
402 do they comply with current legislation? Currently, the EU Directive on ambient air quality and  
403 cleaner air for Europe (22) allows for two types of data in addition to data from reference stations:  
404 indicative measurements and model estimates. For indicative measurements, the EU Directive  
405 requires a minimum of time coverage of 14% (i.e., at least one measurement a week at random,  
406 evenly distributed over the year, or eight weeks evenly distributed over the year). Data collected

407 within citizen science projects (e.g. in a single 4-week campaign) typically do not meet this  
408 criterion, and so they cannot qualify as indicative measurements.

409 In essence, the annual averaged NO<sub>2</sub> data derived from our extrapolation procedure are model  
410 estimates. However, the legal status of these data is uncertain, because it is not clear whether they  
411 comply with the strict definition of “model estimates” as described in the EU Directive. This is  
412 because the EU Directive currently adopts a different view on the usage of models, which does not  
413 include the model approach adopted here. When the EU Directive considers “model approaches”,  
414 the underlying idea is that datasets are available with high temporal resolution and low spatial  
415 resolution (as generated by reference networks), and that geo-spatial, LUR or transport models are  
416 used to perform spatial interpolation (see article 6, paragraph 2 in the EU Directive :“provide  
417 adequate information on the spatial distribution”). Here however, we tackle the opposite problem:  
418 citizen science typically generates datasets that have high spatial resolution (thousands of  
419 participants) but low temporal coverage (only a few weeks). As a consequence, one needs a model  
420 approach that performs temporal extrapolation: passive sampler data collected over a measuring  
421 period of weeks need to be extrapolated to annual averaged values.

422 The emergence of large-scale air quality datasets from citizen science, as discussed here, is a  
423 recent phenomenon and hence it is not surprising that the existing legislation does not properly  
424 accommodate these particular data types. Future legal guidelines may include additional data types  
425 and model protocols, provided they can demonstrate suitable compliance with quality standards.  
426 Our results here demonstrate that citizen derived annual averaged NO<sub>2</sub> data do meet the stringent  
427 data quality criteria imposed the current EU directive, which requires a maximal model uncertainty  
428 of 30%. Based on the deviation for a 4-week period extrapolation using the orthogonal regression  
429 in **Table 1** (2.2 – 2.8 µg/m<sup>3</sup>), the model uncertainty at 40 µg/m<sup>3</sup> (the current WHO and EU limit

430 for annual averages) is 9-11%, which is well below the quality criterion of 30% imposed by the  
431 EU Directive.

432 In summary, short term but spatially extensive measurements campaigns through citizen science  
433 provide an important new data resource, complementing data from official reference networks.  
434 While the existing air quality legislation is currently not well adapted to accommodate these  
435 spatially distributed data with short-term coverage, our results demonstrate that reliable statistical  
436 model extrapolation approaches exist that comply with stringent quality standards. Accordingly,  
437 we propose that future air quality legislation should explicitly consider the existence and use of  
438 these data types and model approaches, and in this way, citizen-derived data could directly feed  
439 into air quality policy. As it happens, the prospect of producing data that are useful to society and  
440 policy is an important motivation for citizens to participate in citizen science projects **(18)**.

## 441 Acknowledgements

442 This work was supported by funding for the citizen science project CurieuzeNeuzen Vlaanderen.  
443 We thank the Prof. R. Blust at University of Antwerp, M. Naert at the newspaper De Standaard  
444 and Mr. M. Van Peteghem at Vlaamse Milieumaatschappij for enabling the CurieuzeNeuzen  
445 project, and all 20.000 citizens for data collection. We thank Huib Huyse for help with the data  
446 collection design and Joris van den Bossche for conceptual input at the early stage of model  
447 development.

## 448 5. References

449 (1) WHO. *Ambient Air Pollution: A Global Assessment of Exposure and Burden of Disease*; Geneva,  
450 Switzerland, 2016.

- 451 (2) Gulia, S.; Shiva Nagendra, S. M.; Khare, M.; Khanna, I. Urban Air Quality Management-A Review.  
452 *Atmos. Pollut. Res.* **2014**, *6* (2), 286–304. <https://doi.org/10.5094/apr.2015.033>.
- 453 (3) Vardoulakis, S.; Solazzo, E.; Lumbreras, J. Intra-Urban and Street Scale Variability of BTEX, NO<sub>2</sub> and  
454 O<sub>3</sub> in Birmingham, UK: Implications for Exposure Assessment. *Atmos. Environ.* **2011**, *45* (29), 5069–  
455 5078. <https://doi.org/10.1016/J.ATMOSENV.2011.06.038>.
- 456 (4) Cyrus, J.; Eeftens, M.; Heinrich, J.; Ampe, C.; Armengaud, A.; Beelen, R.; Bellander, T.; Beregszaszi,  
457 T.; Birk, M.; Cesaroni, G.; et al. Variation of NO<sub>2</sub> and NO<sub>x</sub> concentrations between and within 36  
458 European Study Areas: Results from the ESCAPE Study. *Atmos. Environ.* **2012**, *62* (2), 374–390.  
459 <https://doi.org/10.1016/j.atmosenv.2012.07.080>.
- 460 (5) Wu, H.; Reis, S.; Lin, C.; Beverland, I. J.; Heal, M. R. Identifying Drivers for the Intra-Urban Spatial  
461 Variability of Airborne Particulate Matter Components and Their Interrelationships. *Atmos.*  
462 *Environ.* **2015**, *112*, 306–316. <https://doi.org/10.1016/J.ATMOSENV.2015.04.059>.
- 463 (6) Lin, C.; Feng, X.; Heal, M. R. Temporal Persistence of Intra-Urban Spatial Contrasts in Ambient NO<sub>2</sub>,  
464 O<sub>3</sub> and Ox in Edinburgh, UK. *Atmos. Pollut. Res.* **2016**, *7* (4), 734–741.  
465 <https://doi.org/10.1016/j.apr.2016.03.008>.
- 466 (7) Vardoulakis, S.; Gonzalez-Flesca, N.; Fisher, B. E. A.; Pericleous, K. Spatial Variability of Air Pollution  
467 in the Vicinity of a Permanent Monitoring Station in Central Paris. *Atmos. Environ.* **2005**, *39* (15  
468 SPEC. ISS.), 2725–2736. <https://doi.org/10.1016/j.atmosenv.2004.05.067>.
- 469 (8) Santiago, J. L.; Martín, F.; Martilli, A. A Computational Fluid Dynamic Modelling Approach to Assess  
470 the Representativeness of Urban Monitoring Stations. *Sci. Total Environ.* **2013**, *454–455*, 61–72.  
471 <https://doi.org/10.1016/j.scitotenv.2013.02.068>.
- 472 (9) Yatkin, S.; Gerboles, M.; Belis, C. A.; Karagulian, F.; Lagler, F.; Barbieri, M.; Borowiak, A.

- 473 Representativeness of an Air Quality Monitoring Station for PM<sub>2.5</sub> and Source Apportionment over  
474 a Small Urban Domain. *Atmos. Pollut. Res.* **2019**. <https://doi.org/10.1016/j.apr.2019.10.004>.
- 475 (10) Hafkenschied, T.; Fromage-Marriette, A.; Goelen, E.; Hangartner, M.; Pfeffer, U.; Plaisance, H.; De  
476 Santis, F.; Saunders, K.; Swaans, W.; Tang, S.; et al. *Review of the Application of Diffusive Samplers*  
477 *for the Measurement of Nitrogen Dioxide in Ambient Air in the European Union*; 2009.
- 478 (11) Kracht, O.; Santiago, J. L.; Martin, F.; Piersanti, A.; Cremona, G.; Vitali, L.; Delaney, K.; Basu, B.;  
479 Ghosh, B.; Spangl, W.; et al. *Spatial Representativeness of Air Quality Monitoring Sites - Outcomes*  
480 *of the FAIRMODE/AQUILA Intercomparison Exercise*; 2017. <https://doi.org/10.2760/60611>.
- 481 (12) Palmes, E. D.; Gunnison, A. F.; Dimattio, J.; Tomczyk, C. Personal Sampler for Nitrogen Dioxide. *Am.*  
482 *Ind. Hyg. Assoc. J.* **1976**. <https://doi.org/10.1080/0002889768507522>.
- 483 (13) Gerboles, M.; Buzica, D.; Amantini, L.; Lagler, F.; Hafkenschied, T. Feasibility Study of Preparation  
484 and Certification of Reference Materials for Nitrogen Dioxide and Sulfur Dioxide in Diffusive  
485 Samplers. *J. Environ. Monit.* **2006**, *8* (1), 174–182. <https://doi.org/10.1039/b509559j>.
- 486 (14) Cape, J. N. The Use of Passive Diffusion Tubes for Measuring Concentrations of Nitrogen Dioxide  
487 in Air. *Crit. Rev. Anal. Chem.* **2009**, *39* (4), 289–310. <https://doi.org/10.1080/10408340903001375>.
- 488 (15) Weissert, L. F. F.; Salmond, J. A. A.; Miskell, G.; Alavi-Shoshtari, M.; Williams, D. E. E.; Weissert, L.  
489 F. F.; Williams, D. E. E.; Alavi-Shoshtari, M.; Miskell, G.; Salmond, J. A. A.; et al. Development of a  
490 Microscale Land Use Regression Model for Predicting NO<sub>2</sub> concentrations at a Heavy Trafficked  
491 Suburban Area in Auckland, NZ. *Sci. Total Environ.* **2018**, *619–620*, 112–119.  
492 <https://doi.org/10.1016/j.scitotenv.2017.11.028>.
- 493 (16) Caballero, S.; Esclapez, R.; Galindo, N.; Mantilla, E.; Crespo, J. Use of a Passive Sampling Network  
494 for the Determination of Urban NO<sub>2</sub> Spatiotemporal Variations. *Atmos. Environ.* **2012**, *63*, 148–

- 495 155. <https://doi.org/10.1016/j.atmosenv.2012.08.071>.
- 496 (17) Lebret, E.; Briggs, D.; Van Reeuwijk, H.; Fischer, P.; Smallbone, K.; Harssema, H.; Kriz, B.; Gorynski,  
497 P.; Elliott, P. Small Area Variations in Ambient NO<sub>2</sub> Concentrations in Four European Areas. *Atmos.*  
498 *Environ.* **2000**, *34* (2), 177–185. [https://doi.org/10.1016/S1352-2310\(99\)00292-7](https://doi.org/10.1016/S1352-2310(99)00292-7).
- 499 (18) Van Brussel, S.; Huyse, H. Citizen Science on Speed? Realising the Triple Objective of Scientific  
500 Rigour, Policy Influence and Deep Citizen Engagement in a Large-Scale Citizen Science Project on  
501 Ambient Air Quality in Antwerp. *J. Environ. Plan. Manag.* **2018**, No. February, 1–18.  
502 <https://doi.org/10.1080/09640568.2018.1428183>.
- 503 (19) Haklay, M.; Eleta, I. On the Front Line of Community-Led Air Quality Monitoring. In *Integrating*  
504 *Human Health into Urban and Transport Planning: A Framework*; 2018.  
505 [https://doi.org/10.1007/978-3-319-74983-9\\_27](https://doi.org/10.1007/978-3-319-74983-9_27).
- 506 (20) Irwin, A. No PhDs Needed: How Citizen Science Is Transforming Research. *Nature*. 2018.  
507 <https://doi.org/10.1038/d41586-018-07106-5>.
- 508 (21) Heal, M. R.; Laxen, D. P. H.; Marner, B. B. Biases in the Measurement of Ambient Nitrogen Dioxide  
509 (NO<sub>2</sub>) by Palmes Passive Diffusion Tube: A Review of Current Understanding. *Atmosphere (Basel)*.  
510 **2019**, *10* (7), 357. <https://doi.org/10.3390/atmos10070357>.
- 511 (22) European Commission. Directive 2008/50/EC of the European Parliament and of the Council of 21  
512 May 2008 on Ambient Air Quality and Cleaner Air for Europe. Brussels, Belgium 2008.
- 513 (23) WHO. WHO Air Quality Guidelines for Particulate Matter, Ozone, Nitrogen Dioxide and Sulfur  
514 Dioxide. *World Heal. Organ.* **2005**, *WHO/SDE/PH* (Global update 2005), 5–18.
- 515 (24) Eeftens, M.; Beelen, R.; Fischer, P.; Brunekreef, B.; Meliefste, K.; Hoek, G. Stability of Measured

- 516 and Modelled Spatial Contrasts in NO<sub>2</sub> over Time. *Occup. Environ. Med.* **2011**, *68* (10), 765–770.  
517 <https://doi.org/10.1136/oem.2010.061135>.
- 518 (25) Cesaroni, G.; Porta, D.; Badaloni, C.; Stafoggia, M.; Eeftens, M.; Meliefste, K.; Forastiere, F. Nitrogen  
519 Dioxide Levels Estimated from Land Use Regression Models Several Years Apart and Association  
520 with Mortality in a Large Cohort Study. *Environ. Heal.* **2012**, *11* (1), 48.  
521 <https://doi.org/10.1186/1476-069X-11-48>.
- 522 (26) Wang, R.; Henderson, S. B.; Sbihi, H.; Allen, R. W.; Brauer, M. Temporal Stability of Land Use  
523 Regression Models for Traffic-Related Air Pollution. *Atmos. Environ.* **2013**, *64*, 312–319.  
524 <https://doi.org/10.1016/j.atmosenv.2012.09.056>.
- 525 (27) Carslaw, D. C.; Ropkins, K. Openair --- an R Package for Air Quality Data Analysis. *Environ. Model.*  
526 *Softw.* **2012**, *27–28*, 52–61.
- 527 (28) Manuilova, E.; Schuetzenmeister, A.; Model, F. Mcr: Method Comparison Regression. R Package  
528 Version 1.2.1. 2014.
- 529 (29) Tibshirani, R.; Leisch, F. Bootstrap: Functions for the Book “An Introduction to the Bootstrap”. R  
530 Package Version 2019.6. 2019.
- 531 (30) Denby, B.; Larssen, S. Guidance on the Use of Models for the European Air Quality Directive  
532 (ETC/ACC Version 6.2). *Fairmode* **2010**, 1–99.
- 533 (31) Thunis, P.; Pederzoli, A.; Pernigotti, D. Performance Criteria to Evaluate Air Quality Modeling  
534 Applications. *Atmos. Environ.* **2012**, *59*, 476–482.  
535 <https://doi.org/10.1016/j.atmosenv.2012.05.043>.
- 536 (32) Pyper, B. J.; Peterman, R. M. Comparison of Methods to Account for Autocorrelation in Correlation

537 Analyses of Fish Data. **1998**, 2140, 2127–2140.

538 (33) Henschel, S.; Le Tertre, A.; Atkinson, R. W.; Querol, X.; Pandolfi, M.; Zeka, A.; Haluza, D.; Analitis,  
539 A.; Katsouyanni, K.; Bouland, C.; et al. Trends of Nitrogen Oxides in Ambient Air in Nine European  
540 Cities between 1999 and 2010. *Atmos. Environ.* **2015**, 117, 234–241.  
541 <https://doi.org/10.1016/j.atmosenv.2015.07.013>.

542 (34) Greenpeace. *Mijn Lucht, Mijn School*; 2018.

543 (35) Thunis, P.; Miranda, A.; Baldasano, J. M.; Blond, N.; Douros, J.; Graff, A.; Janssen, S.; Juda-Rezler,  
544 K.; Karvosenoja, N.; Maffei, G.; et al. Overview of Current Regional and Local Scale Air Quality  
545 Modelling Practices: Assessment and Planning Tools in the EU. *Environ. Sci. Policy* **2016**, 65, 13–21.  
546 <https://doi.org/10.1016/j.envsci.2016.03.013>.

547 (36) Henderson, S. B.; Beckerman, B.; Jerrett, M.; Brauer, M. Application of Land Use Regression to  
548 Estimate Long-Term Concentrations of Traffic-Related Nitrogen Oxides and Fine Particulate  
549 Matter. *Environ. Sci. Technol.* **2007**, 41 (7), 2422–2428. <https://doi.org/10.1021/es0606780>.

550 (37) Hoek, G.; Beelen, R.; de Hoogh, K.; Vienneau, D.; Gulliver, J.; Fischer, P.; Briggs, D. A Review of Land-  
551 Use Regression Models to Assess Spatial Variation of Outdoor Air Pollution. *Atmos. Environ.* **2008**,  
552 42 (33), 7561–7578. <https://doi.org/10.1016/j.atmosenv.2008.05.057>.

553 (38) Lewné, M.; Cyrus, J.; Meliefste, K.; Hoek, G.; Brauer, M.; Fischer, P.; Gehring, U.; Heinrich, J.;  
554 Brunekreef, B.; Bellander, T. Spatial Variation in Nitrogen Dioxide in Three European Areas. *Sci.*  
555 *Total Environ.* **2004**, 332 (1–3), 217–230. <https://doi.org/10.1016/j.scitotenv.2004.04.014>.

556

# 1 1. Supplementary methods

## 2 1.1. Data processing and handling of missing data

3 For the 67 stations in the “monitor” dataset, we used 3 different models to describe the relation  
4 between monthly-averaged values  $X_i^R$  and yearly-averaged values  $Y_i^R$  for a subset of stations, and  
5 then applied these models to calculate the yearly-averaged concentrations  $Y_j^{R, \text{model}}$  for an  
6 independent subset of stations. We subsequently compared the model estimates  $Y_j^{R, \text{model}}$  to the  
7 “true” yearly-averaged values  $Y_j^{R, \text{true}}$  that were obtained by direct averaging of the monitoring  
8 data. Furthermore, we determined the uncertainty associated with each regression approach and  
9 investigated the impact of the specific time averaging window ( $T = 2, 4, 6$  and  $8$  weeks) used for  
10 the independent variables  $X_i^R$ .

11 For the “monitor” dataset, day-averaged  $\text{NO}_2$  values were calculated from hourly monitor data at  
12 each individual reference station. Day-averaged values were coded as missing when less than 75%  
13 of the hourly data were available. Time-averaged  $X_i^R$  values were calculated from day-averaged  
14 data for distinct time periods ( $T = 2, 4, 6$  and  $8$  weeks) and were coded as missing when  $<75\%$  of  
15 the daily data was present. Year-averaged  $Y_i^R$  values were also calculated from day-averaged data  
16 and were coded as missing when  $<90\%$  of the daily data were available.

17 For each of the 24 stations in the “sampler” dataset, we extrapolated the sampler data  $X_j^S$  from  
18 different sampling periods to yearly-averaged  $Y_j^S$ . To this end, we first performed a regression  
19 model between the biweekly-averaged  $X_i^R$  values and yearly-averaged  $Y_i^R$  values for the 24  
20 reference monitoring stations at which the samplers were co-located. We then applied this model  
21 to the measured sampler concentrations  $X_j^S$  to arrive at model estimates  $Y_j^{S, \text{model}}$ . Because we have  
22 a full annual cycle of passive sampler measurements, we can compare the model estimates  $Y_j^{S, \text{model}}$

23 to the true yearly averaged sampler data  $Y_j^{S, \text{true}}$ . Subsequently, we investigated the largest  
24 deviations between modeled  $Y_j^{S, \text{model}}$  and measured  $Y_j^{S, \text{true}}$  yearly averages.

25 For the “sampler” dataset, bi-weekly sampler data were either used as such, or averaged over  
26 longer time periods ( $T = 4, 6$  and  $8$  weeks).  $X_j^S$  values were set as missing when one or more of  
27 the bi-weekly measurements were missing. Yearly averaged  $Y_j^S$  values were coded as missing  
28 when  $<75\%$  of the data were available (not counting periods 4 and 5 for which no sampler data  
29 were available).

## 30 1.2 Model development

31 Three different models were tested: orthogonal regression, constant off-set and ratio  
32 multiplication:

$$33 \quad Y_i = a * X_i + b \quad (1)$$

$$34 \quad Y_i = X_i + c \quad (2)$$

$$35 \quad Y_i = r * X_i \quad (3)$$

36 In the orthogonal regression model, the slope  $a$  and intercept  $b$  were calculated using Deming  
37 regression using the ‘mcreg’ function in the R package ‘mcr’ (28), assuming equal uncertainties  
38 for  $X_i$  and  $Y_i$ . The parameter  $c$  in the constant off-set model was determined as the mean of all  
39 individual offsets

$$40 \quad c = \frac{1}{n} \sum_{i=1}^n (Y_i - X_i) \quad (4)$$

41 In the ratio multiplication model, the parameter  $r$  was determined as the mean of the individual  
42 ratios for all stations

43 
$$r = \frac{1}{n} \sum_{i=1}^n \left( \frac{Y_i}{X_i} \right) \quad (5)$$

44

45 **Model application on monitoring data**

46 We used the above 3 models (M = regression, offset, ratio) to describe the relation between the  
 47 multi-week-averages  $X_{i,p}^R$  (averaging period length  $T = 2, 4, 6$  or  $8$  weeks) and the associated  
 48 annual averaged values  $Y_{i,p}^R$ . The subscript  $i$  denotes the specific station ( $i = 1..N_R$ ), while  $p$   
 49 denotes the specific time period ( $p=1..n$ ; the total time series is covered by  $n$  periods of length  $T$ ).

50 We used the jackknife or leave-one-out (LOO) method to estimate the model error, implementing  
 51 the ‘jackknife’ function from the R package ‘bootstrap’ (29). For a given station  $i$  and a given  
 52 period  $p$ , we predicted first the annual average  $Y_{i,p}^{R,model}$  by implementing a given model to the  
 53 data for all other  $N_p^R - 1$  stations (hence excluding station  $i$ ). The residual is then defined as the  
 54 difference between the model value and the true value as directly calculated from the data series

55 
$$\varepsilon_{i,p}^R(T, M) = Y_{i,p}^{R,model}(T, M) - Y_i^{R,true} \quad (6)$$

56 The model error for the period  $p$  is then calculated as the Root Mean Square Error over all stations,  
 57 i.e., the standard deviation of the residuals

58 
$$\sigma_p^R(T, M) = \sqrt{\frac{1}{N_R} \sum_i \varepsilon_{i,p}^R(T, M)^2} \quad (7)$$

59 The model error is dependent upon a specific period  $p$ , a specific model  $M$  and a specific averaging  
 60 period length  $T$ . We can subsequently define the *overall model error* as the Root Mean Square  
 61 Error over all stations for all periods

62 
$$\sigma^R(T, M) = \sqrt{\frac{1}{nN_R} \sum_p \sum_i \varepsilon_{ip}^R(T, M)^2} \quad (8)$$

63 This way, we can compare the model errors for different models M and different averaging period  
 64 lengths T.

65 **Model application on passive sampler data**

66 The 3 models (M = regression, offset, ratio) were applied in a similar way as above. The only  
 67 difference is that models are derived from an independent dataset (i.e., the  $X_i^R$  and  $Y_i^R$  at the  
 68 monitoring stations where samplers are co-located), and so we do not need to use the leave-one-  
 69 out (LOO) method. The residual is now directly defined as the difference between the model  
 70 estimate and the true value at the sampler station as calculated from the sampler data series

71 
$$\varepsilon_{i,p}^S(T, M) = Y_{i,p}^{S,model}(T, M) - Y_i^{S,true} \quad (9)$$

72 The overall model error becomes

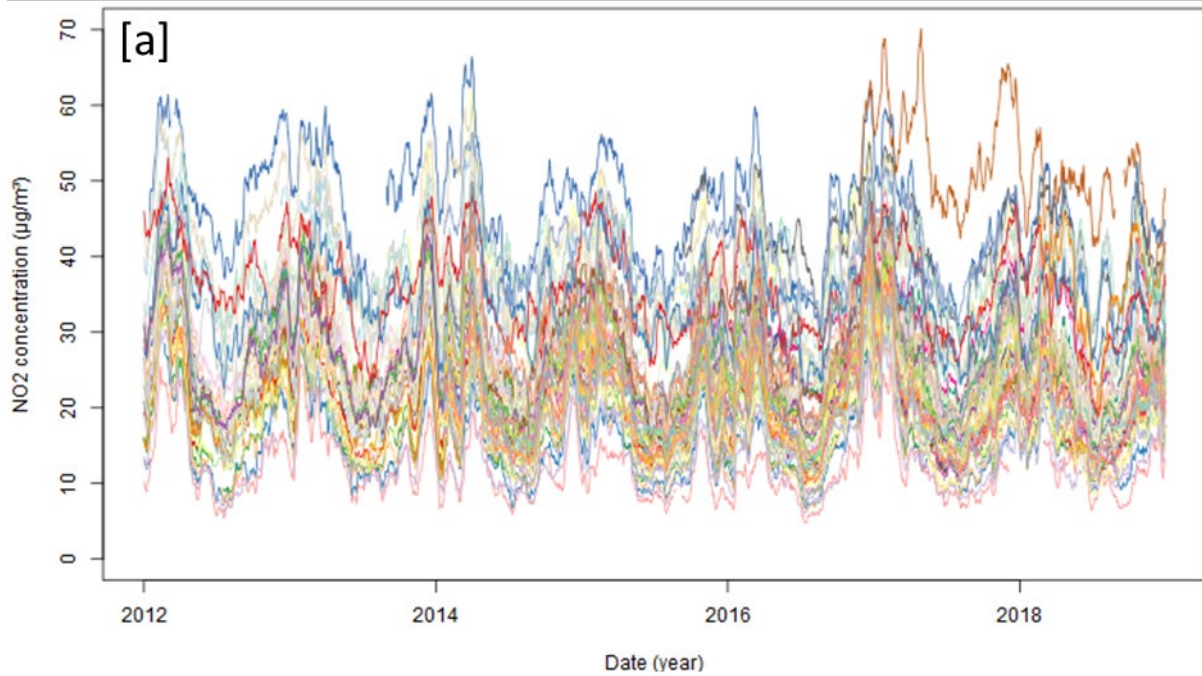
73 
$$\sigma^S(T, M) = \sqrt{\frac{1}{nN_S} \sum_p \sum_i \varepsilon_{ip}^S(T, M)^2} \quad (10)$$

74

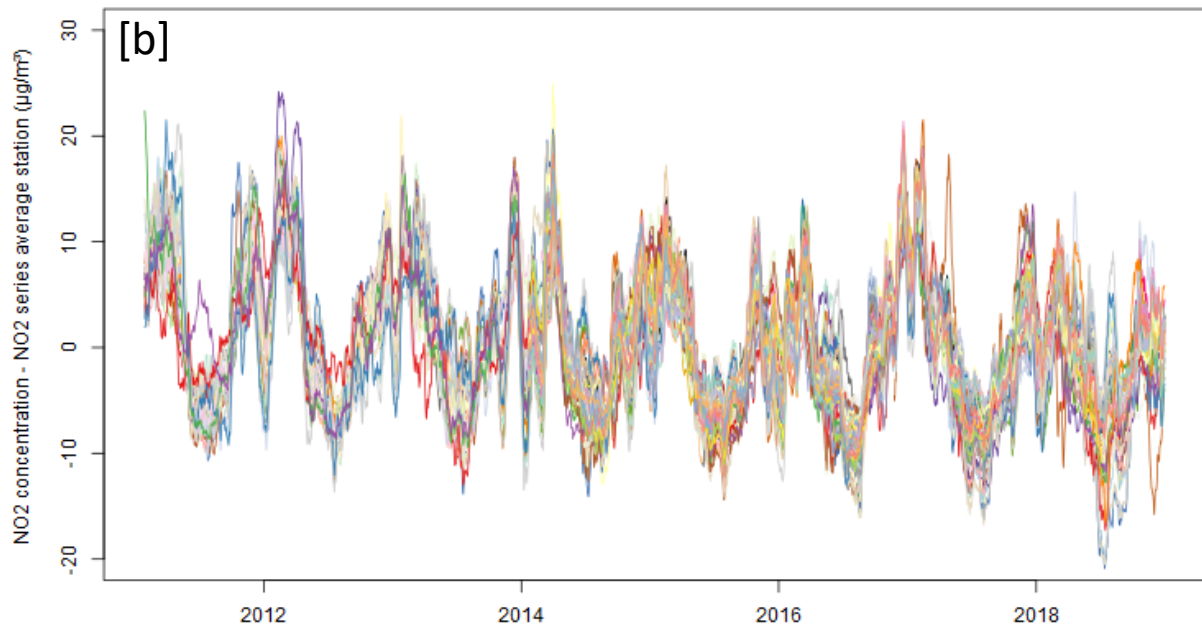
75 [2. Supplementary figures](#)

76

77

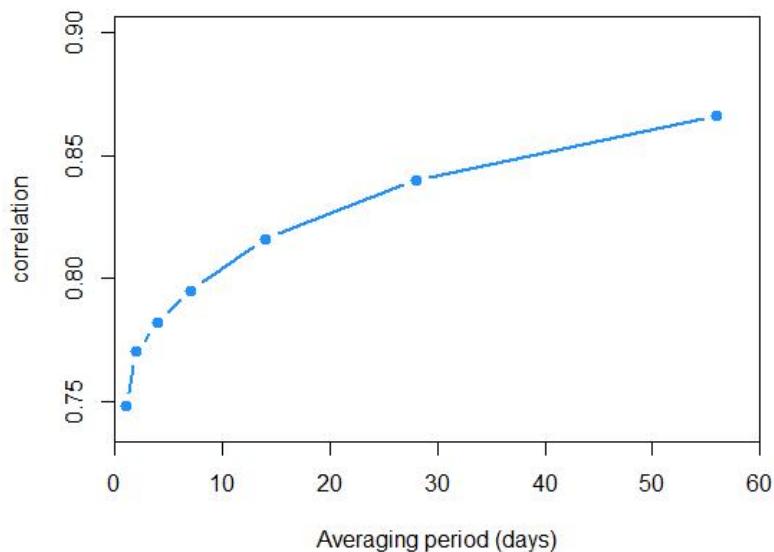


78



79  
80  
81  
82  
83  
84

**Figure S1.** Temporal variation in  $\text{NO}_2$  concentration for the official reference monitoring in Flanders (Belgium). The curves denote 4-week moving averages of hourly  $\text{NO}_2$  data. [a]  $\text{NO}_2$  time series over 8 consecutive years at all 67 stations of the monitoring network. [b] The same time series, but normalized. For each station, the mean  $\text{NO}_2$  concentration over the 8 year period is subtracted. All 67 stations display a similar seasonal pattern and slowly decreasing trend with time.



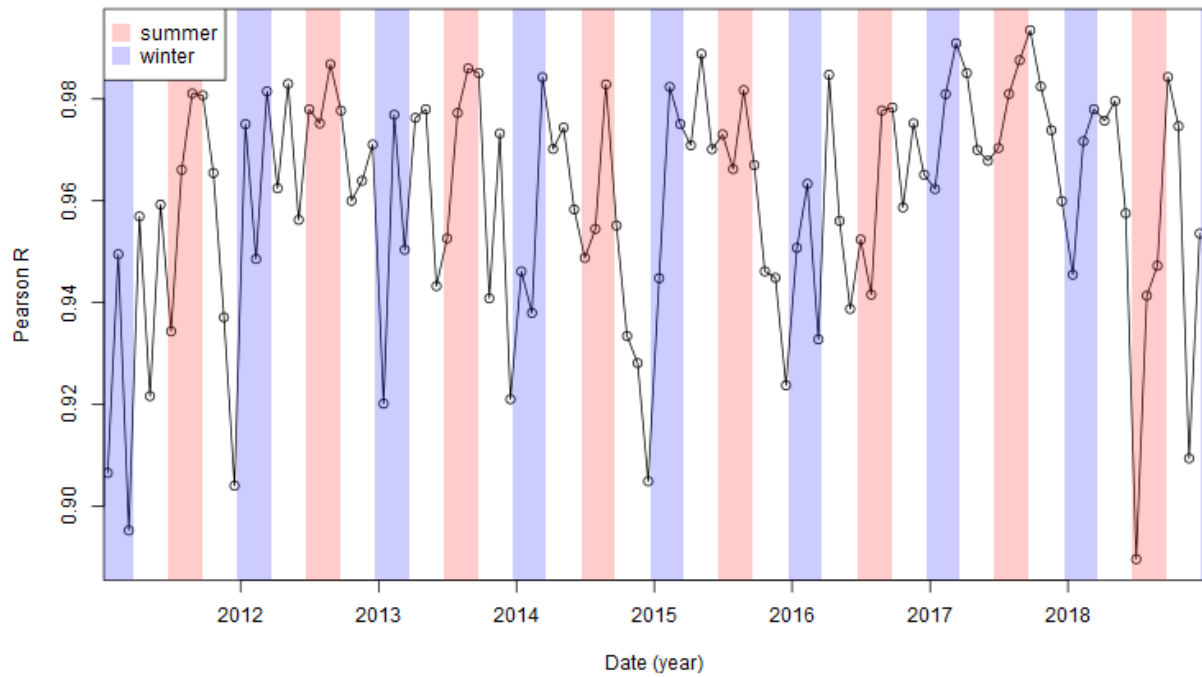
85

86 **Figure S2.** Time series analysis of the NO<sub>2</sub> time series for all 67 stations in the official reference monitoring  
87 in Flanders (Belgium). A pair-wise comparison of the time series of the stations is performed after  
88 application of a moving averaging filter (we restricted the analysis to station pairs that had at least 13  
89 months of overlapping data). The average Pearson correlation R across all 1934 station pairs is plotted as  
90 a function of the moving averaging period. The time series become more correlated as the averaging period  
91 increases.

92

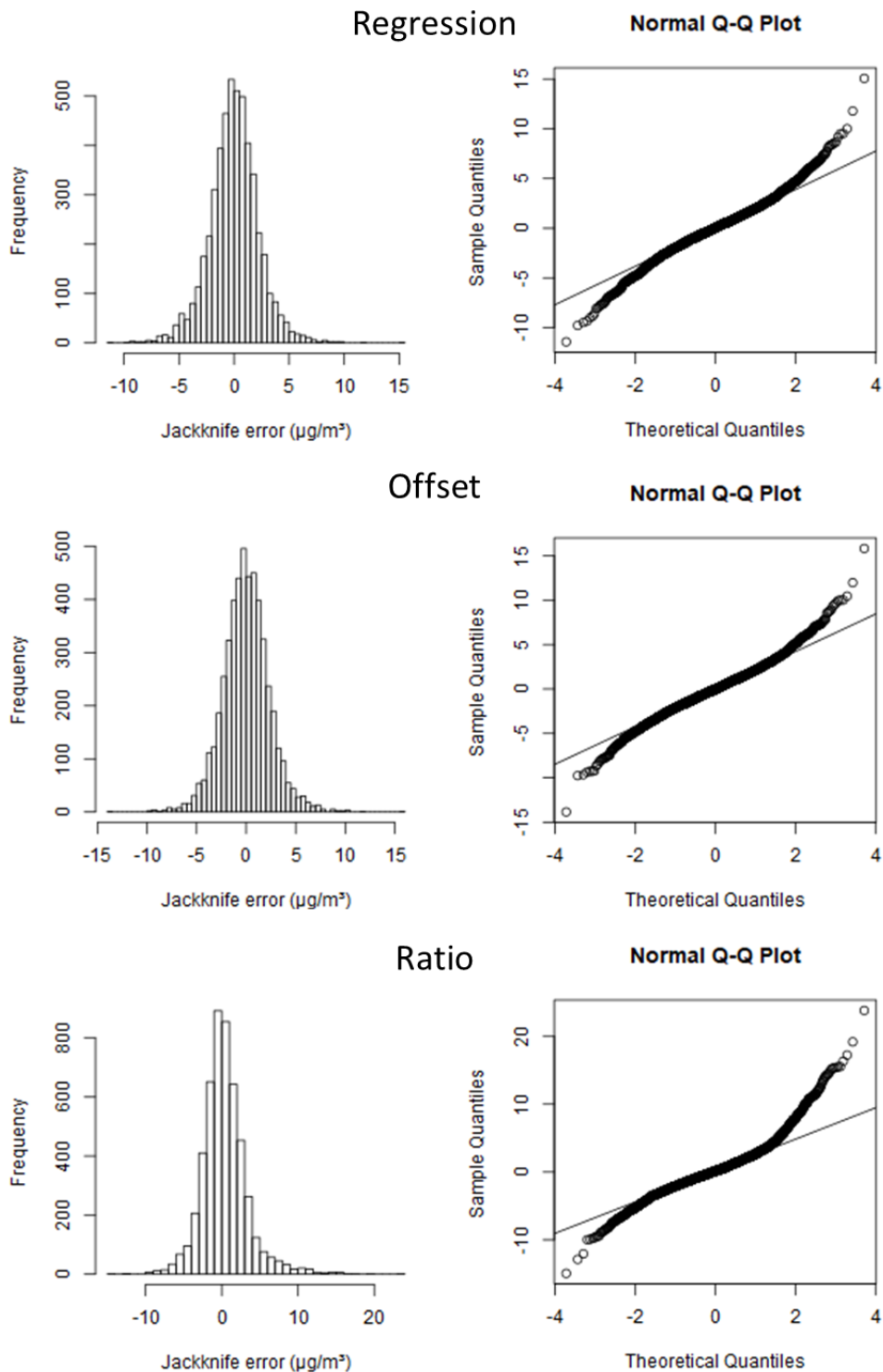
93

94

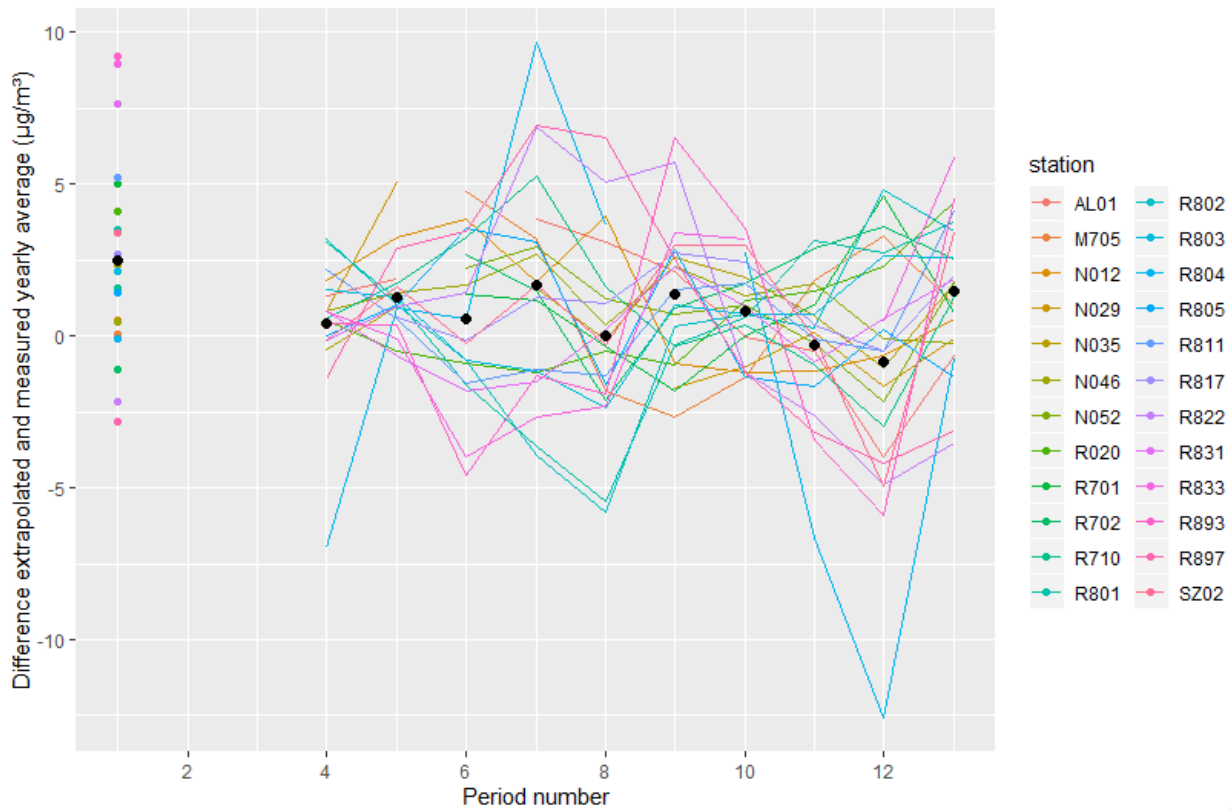


95

96 **Figure S3.** Temporal variation in the Pearson R correlation between monthly and yearly NO<sub>2</sub> data from  
 97 the official reference monitoring in Flanders (Belgium). The correlation is systematically high (>90%).  
 98 The data are displayed per 4 week period. Winter (December 21 to March 20) and summer (June 21 to  
 99 September 20) periods are shown in respectively blue and red shading.



100 **Figure S4.** Histogram and Q-Q plots of residuals obtained by analysis of the monitor dataset. Residuals  
 101 (Jackknife errors) as determined by Eq (6) in the main text through application of the Leave-One-Out  
 102 procedure to model extrapolation from the 4-week periods to year averaged NO<sub>2</sub> values. The results are  
 103 displayed for three different models (regression, offset and ratio) are displayed.

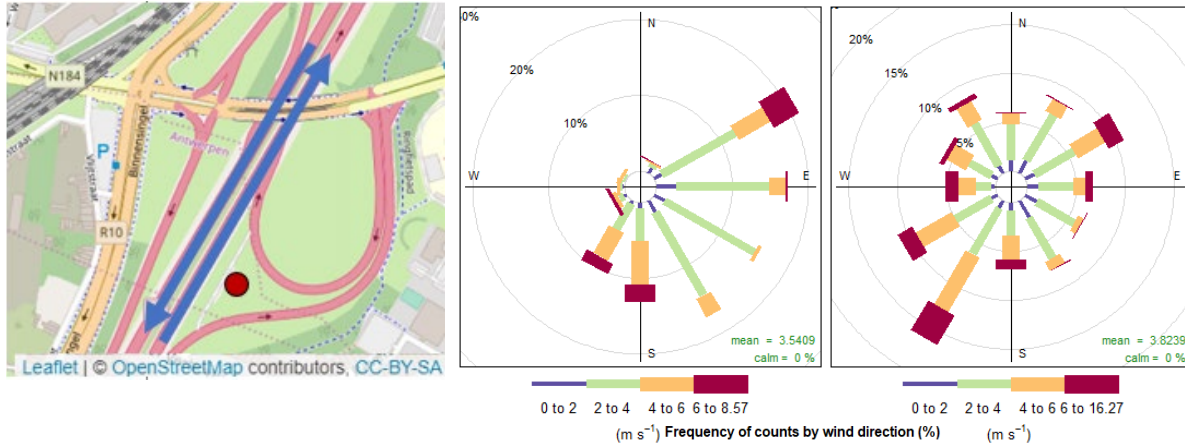


105

106 **Figure S5.** Residuals for the sampler dataset (i.e. the difference between modelled and measured yearly  
 107 averaged  $NO_2$  values as calculated by Eq(10) in the main text). Residuals are displayed per 4-week period  
 108 over the year 2018. Black dots denote the average values per period for all stations. Residuals from periods  
 109 2 and 3 are missing due to absence of sampler data .

110

111



112

113 **Figure S6.** The highway station R804 shows a high model error over period 12 in 2018. [a] Location of  
 114 highway station R804 (red dot) and local traffic flows (blue arrows). [b] Wind rose only for period 12 in  
 115 2018 [c] Wind rose for the whole of 2018. Colors show fraction of winds at a certain wind speed for each  
 116 direction.

117